Assimilation and Simulation of Typhoon Rusa (2002) Using the WRF System

GU Jianfeng[*1,2,3] (顾建峰), Qingnong XIAO[2], Ying-Hwa KUO[2], Dale M. BARKER[2],

XUE Jishan[1] (薛纪善), and MA Xiaoxing[3] (马晓星)

[1]*Chinese Academy of Meteorological Sciences, Beijing* 100081

[2]*National Center for Atmospheric Research, Boulder, Colorado* 80307, *USA*

[3]*Shanghai Weather Forecast Center, Shanghai* 200030

ABSTRACT

Using the recently developed Weather Research and Forecasting (WRF) 3DVAR and the WRF model, numerical experiments are conducted for the initialization and simulation of typhoon Rusa (2002). The observational data used in the WRF 3DVAR are conventional Global Telecommunications System (GTS) data and Korean Automatic Weather Station (AWS) surface observations. The Background Error Statistics (BES) via the National Meteorological Center (NMC) method has two different resolutions, that is, a 210-km horizontal grid space from the NCEP global model and a 10-km horizontal resolution from Korean operational forecasts. To improve the performance of the WRF simulation initialized from the WRF 3DVAR analyses, the scale-lengths used in the horizontal background error covariances via recursive filter are tuned in terms of the WRF 3DVAR control variables, streamfunction, velocity potential, unbalanced pressure and specific humidity. The experiments with respect to different background error statistics and different observational data indicate that the subsequent 24-h the WRF model forecasts of typhoon Rusa's track and precipitation are significantly impacted upon the initial fields. Assimilation of the AWS data with the tuned background error statistics obtains improved predictions of the typhoon track and its precipitation.

Key words: 3DVAR, data assimilation, background error statistics, numerical simulation, typhoon

1. Introduction

The problem of determining a physically consistent and accurate snapshot of the atmosphere is central to numerical weather prediction (NWP). Nearly 50 years ago, in the period of scientific excitement and challenge that followed the first successful numerical weather prediction, the variational approach to meteorological analysis was introduced by Sasaki (1958). In succeeding decades, with advances in both computing power and optimization strategies, more sophisticated constraints and more diverse observations have been included in the problem. In the nomenclature of meteorology, this methodology has become known as three-dimensional variational (3DVAR, all space coordinates but excluding time) and four-dimensional variational (4DVAR, when time is included) data assimilation. The adjoint formalism was first proposed by Le Dimet (1982) for meteorological applications and was then implemented by Derber (1985), Lewis and Derber (1985), Courtier (1985), Le Dimet and Talagrand (1986), Talagrand and Courtier (1987), Navon et al. (1992), Zupanski (1993), Zou et al. (1993a, b), Li et al. (2000) and Xiao et al. (2002), among others. However, 4DVAR has been known to be very time-consuming due to the adjoint nature of model integration in iteratively searching for the optimal solution (Li and Navon, 2001). In 3DVAR, since both model integration and adjoint model integration are not needed, it greatly simplifies the filtering processes with relatively cheaper adjoint operators for ingestion of various observations (Rabier et al., 1997; Courtier

---

*E-mail: jfgu@china221.com

Current affiliation: Gu Jianfeng, Shanghai Weather Forecast Center, Shanghai 200030

et al., 1998).

The Weather Research and Forecasting (WRF) project is a multi-institutional effort to develop an advanced mesoscale forecast and data assimilation system that is accurate, efficient, and scalable across a range of scales. The newest version (2.0) of the WRF model and the WRF 3DVAR were released in 2004. The configuration of the WRF 3DVAR system is based on an incremental formulation producing a multivariate incremental analysis in the WRF model space. The incremental cost function minimization is performed in a preconditioned control variable space. The preconditioned control variables we use in this study are stream-function, velocity potential, unbalanced pressure and specific humidity. Balance between mass and wind increments is achieved via a geostrophically and cyclostrophically balanced pressure derived from the wind increments. Statistics of differences between 24 h and 12 h forecasts are used to estimate background error covariances via the National Meteorological Center (NMC) method (Parrish and Derber, 1992). Representation of the horizontal component of background error is via horizontally isotropic and homogeneous recursive filters. The vertical component is applied through projection onto climatologically averaged (in time, longitude, and optionally latitude) eigenvectors of vertical error estimated via the NMC method. Horizontal/vertical errors are nonseparable in that horizontal scales vary with vertical eigenvectors. A detailed description of the 3DVAR system can be found in Barker et al. (2004).

Numerical prediction of tropical cyclones has improved enormously over the past few decades. The difficulties in the numerical prediction of tropical cyclone track, intensity and inner-core structure are associated with insufficient observations over the oceans and with the limitations of numerical models, such as low-resolution, crude physical parameterization, and the inability to treat multiscale interaction. Recently, tropical cyclone forecast models at high resolution have greatly improved as a result of advances in computer resources. More sophisticated models have been developed and used for tropical cyclone study and forecast. To improve the tropical cyclone analysis and to produce an adequate initial condition for prediction becomes an important procedure. In the recent studies of Zou and Xiao (2000), Xiao et al. (2000), and Zhang et al. (2003), the MM5 4DVAR data assimilation method was proposed to generate the structure of a tropical cyclone and the adjacent synoptic features with insufficient observations over the ocean in the initial condition of the high-resolution mesoscale model MM5. The predictions of tropical cyclone track and intensity were improved in their studies.

The main purpose of this paper is to demonstrate the ability of the WRF 3DVAR in analyses of Typhoon Rusa (2002) and its surrounding atmosphere and to assess their impact on the subsequent the WRF model forecasts of the typhoon. The WRF 3DVAR analyses for typhoon initialization are tuned by changing the scale-lengths of horizontal Background Error Statistics (BES). Conventional Global Telecommunication System (GTS) and Korean Automatic Weather Station (AWS) observational data are used to enhance the 3DVAR analyses of the typhoon and surrounding atmosphere. Numerical forecasts of the typhoon track and rainfall are conducted with the WRF model. This paper is organized as follows. The next section briefly describes the WRF 3DVAR and the WRF modeling system. Section 3 gives a synoptic overview of typhoon Rusa (2002). The preprocessing of the conventional GTS and Korean AWS observational data, and the preparation of the WRF 3DVAR first-guess fields using National Centers for Environmental Prediction (NCEP) AVN data and the WRF standard initialization (SI), will be presented in section 4. In section 5, the scale-lengths of the WRF 3DVAR assimilation are tuned based on the root-mean-square errors and the single observation tests. Section 6 will describe our experimental design and list our data assimilation and simulation experiments. In section 7, the numerical simulation results are presented. And finally, the summary and conclusions are given in section 8.

2. Brief description of the WRF 3DVAR and the WRF modeling system

2.1 *The WRF 3DVAR*

The basic goal of the WRF 3DVAR system is to seek an "optimal" estimate of the true atmospheric state at analysis time through iterative solution of a prescribed cost-function:

$$J(\boldsymbol{x}) = \frac{1}{2}(\boldsymbol{x} - \boldsymbol{x}_{\mathrm{b}})^{\mathrm{T}} \boldsymbol{B}^{-1}(\boldsymbol{x} - \boldsymbol{x}_{\mathrm{b}})$$
$$+ \frac{1}{2}(\boldsymbol{y} - \boldsymbol{y}_0)^{\mathrm{T}} \boldsymbol{O}^{-1}(\boldsymbol{y} - \boldsymbol{y}_0). \qquad (1)$$

The problem can be summarized as the iterative solution of Eq. (1) to find the analysis state $\boldsymbol{x}$ that minimizes $J(\boldsymbol{x})$. This solution represents the estimate of the true atmospheric state given the two sources of a priori data: the background (previous forecast) $\boldsymbol{x}_{\mathrm{b}}$ and observations $\boldsymbol{y}_0$ (Lorenc 1986). $\boldsymbol{B}$ and $\boldsymbol{O}$ are the background and observation error covariance matrices respectively. The observation operator $\boldsymbol{H}$ is used to transform the gridded analysis $\boldsymbol{x}$ to observation space $\boldsymbol{y} = \boldsymbol{H}\boldsymbol{x}$ for comparison against observations. One practical solution to this problem is to perform

a preconditioning via a control variable $\boldsymbol{v}$-transform defined by $\delta\boldsymbol{x} = \boldsymbol{U}\boldsymbol{v}$, where $\delta\boldsymbol{x} = \boldsymbol{x} - \boldsymbol{x}_{\mathrm{b}}$. The transform $\boldsymbol{U}$ is chosen to approximately satisfy the relationship $\boldsymbol{B} = \boldsymbol{U}\boldsymbol{U}^{\mathrm{T}}$. Using the incremental formulation (Courtier et al., 1994) and the control variable transform, Eq. (1) can be rewritten as:

$$J(\boldsymbol{v}) = \frac{1}{2}\boldsymbol{v}^{\mathrm{T}}\boldsymbol{v} + \frac{1}{2}(\boldsymbol{d} - \boldsymbol{H}'\boldsymbol{U}\boldsymbol{v})^{\mathrm{T}}\boldsymbol{O}^{-1}(\boldsymbol{d} - \boldsymbol{H}'\boldsymbol{U}\boldsymbol{v}) , \quad (2)$$

where $\boldsymbol{d} = \boldsymbol{y}_0 - \boldsymbol{H}(\boldsymbol{x}_{\mathrm{b}})$ is the innovation vector and $\boldsymbol{H}'$ is the linearization of the potentially nonlinear observation operator.

The "NMC method" (Parrish and Derber, 1992) provides a climatological estimate of background error covariance, assuming it to be well approximated by averaged forecast difference (e.g., month-long series of 24-h minus 12-h forecasts valid at the same time) statistics:

$$\boldsymbol{B} = \overline{(\boldsymbol{x}_{\mathrm{b}} - \boldsymbol{x}_{\mathrm{t}})(\boldsymbol{x}_{\mathrm{b}} - \boldsymbol{x}_{\mathrm{t}})^{\mathrm{T}}} = \overline{\boldsymbol{\varepsilon}_{\mathrm{b}}\boldsymbol{\varepsilon}_{\mathrm{b}}^{\mathrm{T}}}$$
$$\cong \overline{(\boldsymbol{x}_{24} - \boldsymbol{x}_{12})(\boldsymbol{x}_{24} - \boldsymbol{x}_{12})^{\mathrm{T}}} . \quad (3)$$

The control variable transform is in practice composed of a series of operations $\delta\boldsymbol{x} = \boldsymbol{U}_p\boldsymbol{U}_v\boldsymbol{U}_h\boldsymbol{v}$ (Lorenc et al., 2000) ensuring the relationship $\boldsymbol{B} = \boldsymbol{U}_p\boldsymbol{U}_v\boldsymbol{U}_h\boldsymbol{U}_h^{\mathrm{T}}\boldsymbol{U}_v^{\mathrm{T}}\boldsymbol{U}_p^{\mathrm{T}}$. The horizontal component of the background error covariance $\boldsymbol{B}_h = \boldsymbol{U}_h\boldsymbol{U}_h^{\mathrm{T}}$ is performed using recursive filters (Hayden and Purser, 1995; Purser et al., 2003a). The version of the recursive filter used in this paper possesses two free parameters for each control variable: the number of applications N of the filter [$N = 2$ defines a second-order autoregressive (SOAR) function response; as $N \to \infty$, the response approximates a Gaussian] and the correlation scale length s of the filter. The recursive filter (RF) is presented with an initial function A_i at gridpoints i where $1 \leqslant i \leqslant I$. A single pass of the RF consists of an initial smoothing from "left" to "right":

$$B_i = \alpha B_{i-1} + (1 - \alpha)A_i \quad i = 1, 2, \ldots, I \quad (4)$$

followed by a pass from "right" to "left":

$$C_i = \alpha C_{i+1} + (1 - \alpha)B_i \quad i = 1, 2, \ldots, l . \quad (5)$$

Given parameters N, s and Δx, the value of α to be used in the RF algorithm is then

$$\alpha = 1 + E - \sqrt{E(E + 2)} , \quad (6)$$

where

$$E = N(\Delta x)^2/4s^2 . \quad (7)$$

The NMC method is used to derive estimates of the recursive filter's characteristic scale length s that depend on model level streamfunction (Ψ), velocity potential (χ), unbalanced pressure (p_{u}) and specific humidity (q) projected onto their vertical error modes. The vertical component $\boldsymbol{B}_v = \boldsymbol{U}_v\boldsymbol{U}_v^{\mathrm{T}}$ is applied via a projection

from eigenvectors and eigenvalues of a climatological estimate onto model levels, and the physical variable transformation $\boldsymbol{B}_p = \boldsymbol{U}_p\boldsymbol{U}_p^{\mathrm{T}}$ converts control variables to model variables (e.g., u, v, T, p, q).

2.2 *The WRF model*

The WRF model is a next-generation mesoscale model that advances both the understanding and the prediction of mesoscale weather systems and promotes closer ties between the research and operational forecasting communities. The WRF model is intended for a wide range of applications, from idealized research to operational forecasting with priority emphasis on horizontal grids of 1–10 km. It is a joint effort of model development among several organizations, such as the National Center for Atmospheric Research (NCAR), Forecast Systems Laboratory (FSL) of the National Oceanic and Atmospheric Administration (NOAA), Center for the Analysis and Prediction of Storms (CAPS) at the University of Oklahoma, National Aeronautics and Space Administration (NASA), Air Force Weather Agency (AFWA), and a number of collaborating institutes and universities.

The equations are in terms of a terrain-following hydrostatic pressure vertical coordinate:

$$\eta = (p_{\mathrm{h}} - p_{\mathrm{ht}})/\mu , \quad (8)$$

where $\mu = p_{\mathrm{hs}} - p_{\mathrm{ht}}$, p_{h} is the hydrostatic component of the pressure, and p_{hs} and p_{ht} refer to values along the surface and top boundaries, respectively. $\mu(x, y)$ represents the mass per unit area within the column in the model domain, and the appropriate flux form variables are:

$$\boldsymbol{V} = \mu\boldsymbol{v} = (U, V, W) , \quad \boldsymbol{\Omega} = \mu\dot{\eta} , \quad \Theta = \mu\theta . \quad (9)$$

So the prognostic equations are:

$$\partial_t U + (\nabla \cdot \boldsymbol{v}U)_\eta + \mu\alpha\partial_x p + \partial_\eta p\partial_x\phi = F_U , \quad (10)$$

$$\partial_t V + (\nabla \cdot \boldsymbol{v}V)_\eta + \mu\alpha\partial_y p + \partial_\eta p\partial_y\phi = F_V , \quad (11)$$

$$\partial_t W + (\nabla \cdot \boldsymbol{v}W)_\eta - g(\partial_\eta p - \mu) = F_W , \quad (12)$$

$$\partial_t\Theta + (\nabla \cdot \boldsymbol{v}\Theta)_\eta = F_\Theta , \quad (13)$$

$$\partial_t\mu + (\nabla \cdot \boldsymbol{V})_\eta = 0 , \quad (14)$$

$$\partial_t\phi + (\boldsymbol{v} \cdot \nabla\phi)_\eta = gw , \quad (15)$$

$$\partial_\eta\phi = -\mu\alpha , \quad (16)$$

$$p = \left(\frac{R\Theta}{p_0\mu\alpha}\right)^\gamma . \quad (17)$$

The WRF dynamical core uses Eulerian finite-differencing to integrate the fully compressible non-hydrostatic equations in mass-coordinate, scalar-conserving flux form using a time-split small step for acoustic modes. Large time steps utilize a third-order Runge-Kutta technique. The horizontal staggering is

an Arakawa-C grid. The WRF physical processes for real-data mesoscale forecasts include selections of explicit microphysics schemes, cumulus convective parameterizations, planetary boundary layer (PBL) parameterizations, and long-wave and shortwave radiation schemes.

3. Overview of Typhoon Rusa (2002)

Typhoon Rusa was initiated from a tropical wave in the mid-Pacific ocean. On 23 August 2002, Rusa formed as a tropical depression over the Pacific, about 600 km southwest of Wake Island. It tracked towards the west-northwest and strengthened into a tropical storm the same day. Rusa reached typhoon strength on 26 August 2002 and continued to move west-northwestwards over the Pacific Ocean. It then turned to the northwest and skirted the Ryukyu Islands. Rusa turned north on 30 August 2002 and made landfall over South Korea on 31 August at around 0630 UTC.

Rusa was a very strong typhoon with the minimum sea-level pressure of 950 hPa sustained from 0000 UTC 29 till 1200 UTC 30 August 2002. Before landfall on

31 August 2002, the typhoon kept the strength of its central sea-level pressure between 950 and 960 hPa. But it weakened rapidly after landfall and became an extratropical cyclone over the Sea of Japan on the first day of September 2002.

During the final day of August 2002, typhoon Rusa swept past the Japanese island of Kyushu and clobbered South Korea, killing more than 110 people and submerging thousands of homes. Typhoon Rusa was the most disastrous weather system in Korea in 2002. It moved across the country and dumped very heavy rainfall in a short time period. The heavy rainfall of 870 mm d^{-1} at Kangnung city was the highest on record in Korea's 100-year meteorological history. The KMA Jindo radar captured the system before the typhoon landed at the south coast. Figure 1 shows the radar images (rainfall rate) captured by the Jindo radar at about 0000 UTC 31 August 2002. It can be seen that the typhoon structure is well depicted.

0000 UTC 31 August 2002 is selected as the analysis time for assimilation and the initial time for simulation. The observations of conventional GTS and Korea AWS data are assimilated into the WRF 3DVAR analyses to generate the initial conditions at that time.
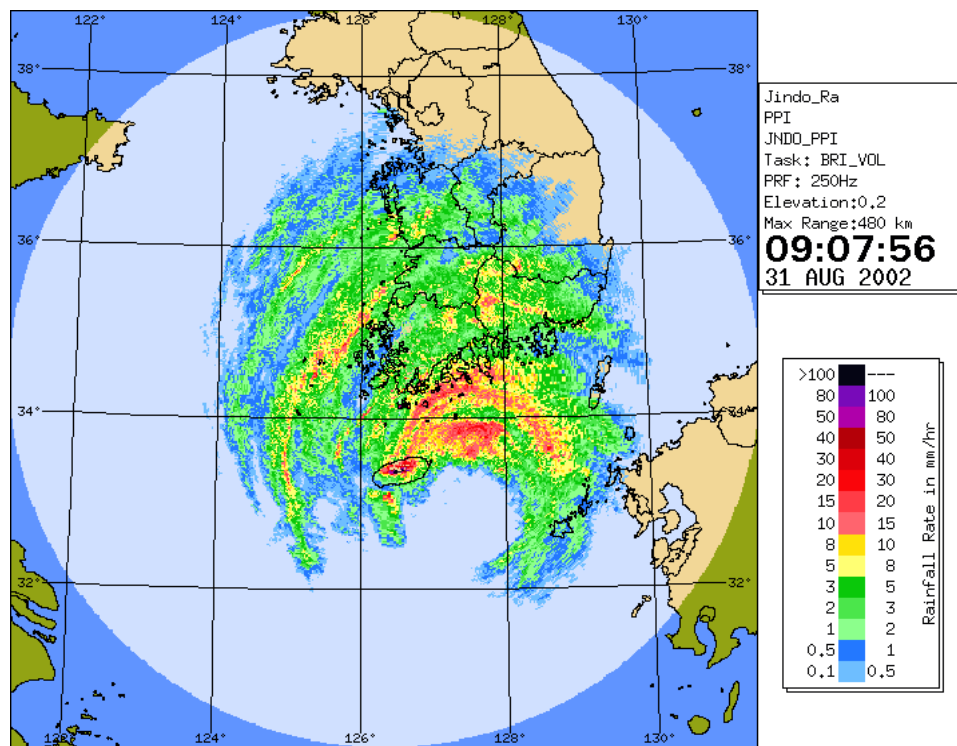

Fig. 1. Korea Jindo radar captured image (rainfall rate) of typhoon Rusa at about 0000 UTC 31 August 2002.

4. Data preprocessing

The domain of the WRF 3DVAR analysis and the WRF model simulation has 178×160 grid points and the center of the domain is located at (37.03°N, 125.13°E). The standard latitudes of the Lambert map projection are 30°N and 60°N. The horizontal resolution is 10 km and the vertical levels are 34 in the WRF model framework.

The domain specification (projection parameters, dimensions, location, etc.) is made in the WRF SI. From this definition, the WRF SI creates the grid specification as well as various static fields such as topography, land use, soil types, monthly greenness fraction, latitudes, longitudes, etc. The WRF REAL program interpolates the NCEP AVN data to the WRF grid in horizontal and vertical space as the analysis, and specifies the lateral boundary conditions. The NCEP AVN analysis data used in this paper are from 0000 UTC 30 August 2002 to 0000 UTC 1 September 2002 with a 6-hour interval. The fields of the WRF model 24 h integration from 0000 UTC 30 August 2002 to 0000 UTC 31 August 2002 provide the background (first guess) for the WRF 3DVAR.

Conventional observations from GTS and AWSs are preprocessed using the WRF 3DVAR observation preprocessor (3DVAR OBSPROC). Because observation errors can be introduced at all stages including measurement, reporting practices, transmission and decoding, it is important that careful quality control (QC) is performed to avoid the assimilation of erroneous observations. In the WRF 3DVAR observation preprocessor, a number of QC checks are performed including the removal of observations outside the time range and domain (horizontal and top), re-ordering and merging the duplicate data reports in time location, retrieving the pressure or height based on the observation information with the hydrostatic assumption, ensuring the vertical consistency and super adiabatic property for multi-level observations, and estimating observational error based on the pre-specified errors. Numerous QC checks are redone in the WRF 3DVAR itself and an "error_max" check is performed to reject observations whose innovation vector $(O-B)$ is greater than 5 times of the assumed observation error standard deviation.

We select 0000 UTC 31 August 2002 as the analysis time for assimilation and as the initial time for simulation. All the assimilation observations in our designed experimental domain are shown in Fig. 2. Totally, the conventional GTS data (Fig. 2a) consist of 197 surface observations (SYNOP, symbol "×"), 28 radiosonde profiles (SOUND, symbol "O") and 6 ship reports (SHIP, symbol "×"). As extra information,

the Korean AWS network provided 490 surface observations (Fig. 2b) in South Korea (AWS, symbol "+").

5. Scale-length tunings of the background error statistics

We have two types of background error statistics (BES) via the NMC method; one is calculated from the NCEP global model with a 210 km horizontal grid distance (global BES), and the other is from the Korean operational MM5 mesoscale model with a 10 km horizontal resolution and identical domain to this study
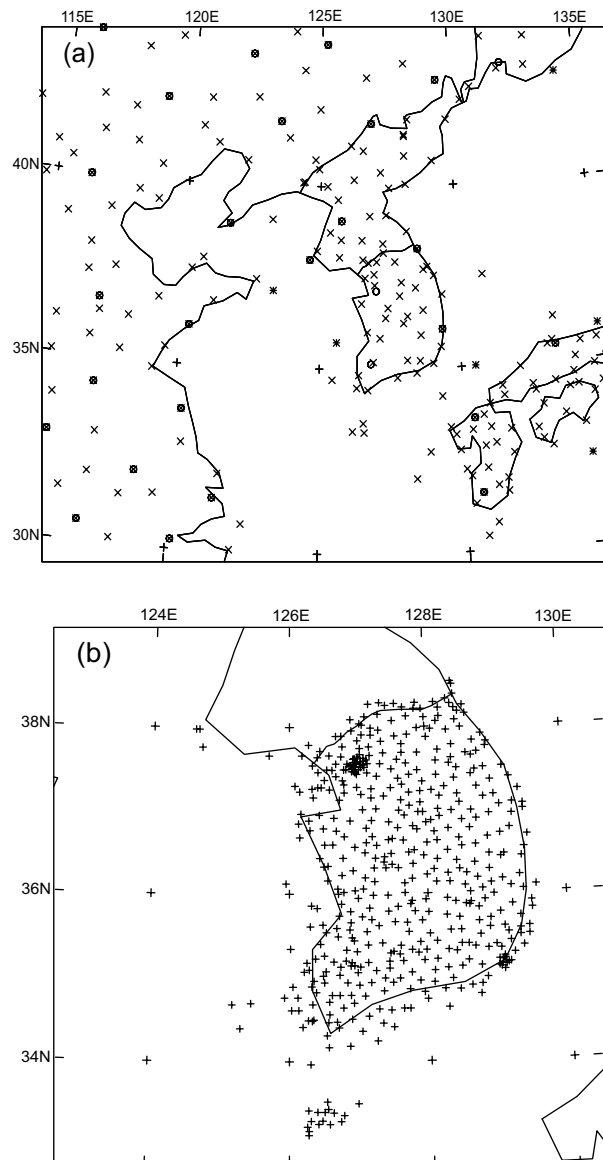

Fig. 2. The assimilation observation data distribution in the domain (a) The SYNOP (×), SOUND (○), and SHIP (∗) observations; (b) The METAR (+) observations in South Korea.
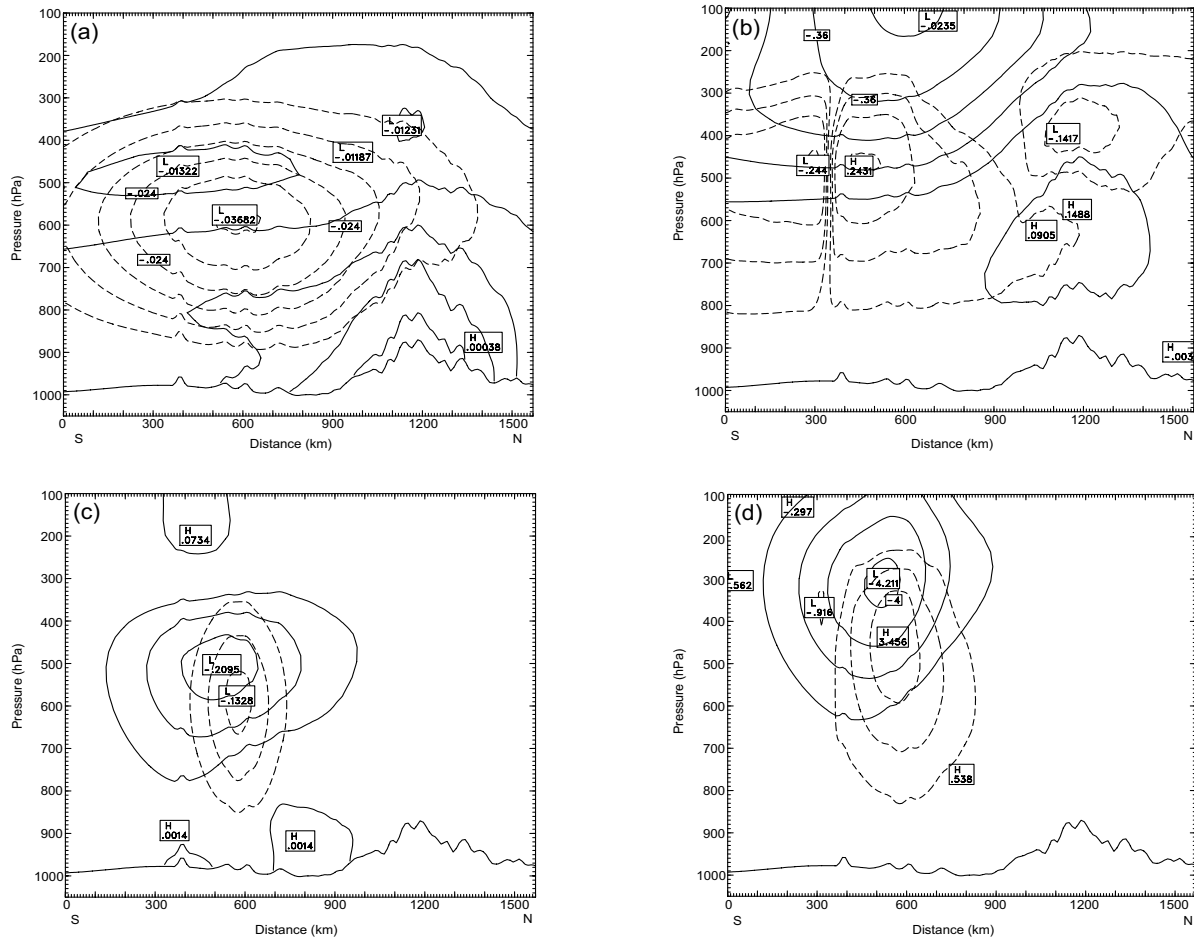
Fig. 3. The increment profiles at a S-N cross section from the WRF 3DVAR with single observation test. (a) The increments of T (solid lines) and q_v (dashed lines) with the default global BES; (b) The increments of ϕ (solid lines) and wind speed (dashed lines) with the default global BES; (c) Same as (a) but with the tuned global BES; (d) Same as (b) but with the tuned global BES.

(MM5 BES). Using the WRF 3DVAR system, we assimilate a single observation at 500 hPa from Kwangju sounding station in Korea (35.11°N, 126.81°E) to inspect its influence scales. Figure 3 shows the increments at the S-N cross section from the WRF 3DVAR analyses with the global BES. As the default, we have an interpolated BES from the global BES. It can be seen that the horizontal influence extension of increments is unreasonable large with the default global BES (Figs. 3a, b).

In order to find an optimal horizontal component of background error covariance $(\boldsymbol{B}_h = \boldsymbol{U}_h \boldsymbol{U}_h^{\mathrm{T}})$ in the WRF 3DVAR system for this case study, one important thing we can do is to tune the BES file. The scale-lengths in the recursive filter can be tuned based on the statistics of the 3DVAR analyses. As Wu et al. (2002) found that the horizontal scales decrease when the resolution of the forecast model is increased,

we apply tuning factors for the scale-lengths of the 3DVAR control variables to the global BES (210-km resolution). Many WRF 3DVAR experiments are conducted, and the root-mean-square errors (RMSEs) of all the 3DVAR analyses compared to the observations are calculated. The statistics indicate that the 3DVAR analyses are reasonably close to the observations with the tuning factors of 0.11, 0.11, 0.11, and 0.45 respectively for the control variables of streamfunction (Ψ), velocity potential (χ), unbalanced pressure (p_u), and the specific humidity (q_v). Figures 3c and 3d present the increments with the tuned global BES. It can be seen that the horizontal influence extension of increments is more reasonable for this typhoon case.

In the same way, we also tuned the scale-lengths of the MM5 BES in our experiments. It is indicated that the tuning factors of 0.5, 0.5, and 0.5 for streamfunction (Ψ), velocity potential (χ) and unbalanced pres-
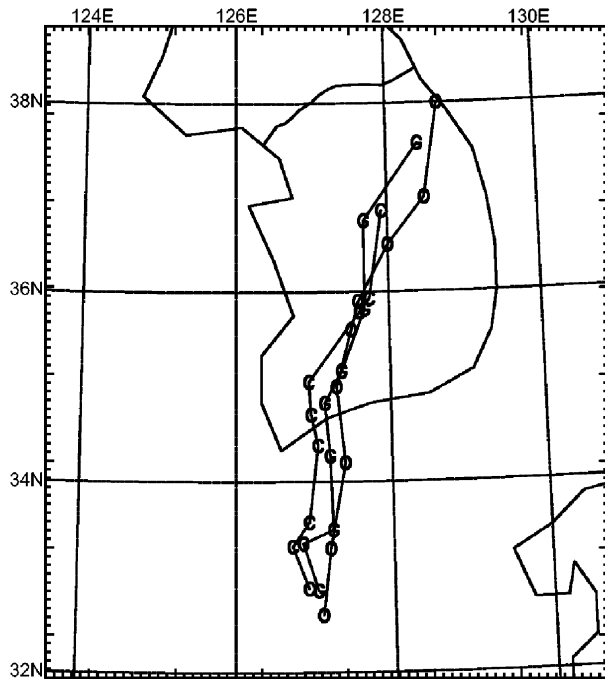
Fig. 4. Typhoon Rusa's simulated and observed tracks. Symbol "O" is the best track; Symbol "C" is the CNTL track; Symbol "G" is the experiment MBESD track.

sure (p_u) give reasonably small RMSEs in the 3DVAR analyses.

6. Experimental design

Totally, seven experiments were designed and carried out according to different BESs and different observational data. The first guess of the WRF 3DVAR is the WRF model 24-h forecast with the NCEP AVN analysis and the WRF SI as the initial condition at 0000 UTC 30 August 2002. The tropical cyclone initialization using the WRF 3DVAR system is conducted at 0000 UTC 31 August 2002. The 7 experiments are listed below:

CNTRL: The control experiment is the WRF model straightforward 24-h forecast starting with the WRF 3DVAR first guess without observational data assimilation;

GBESD: Conventional GTS observation data (Fig. 2a) are assimilated via the WRF 3DVAR with the default global BES (Figs. 3a, b), followed by a 24-h forecast using the WRF model. The first letter "G" represents global and the last letter "D" represents default;

GBESL: Same as GBESD, but the scale-lengths of the global BES are tuned in the WRF 3DVAR (Figs. 3c, d). The last letter "L" represents the tuning of the length factors in the WRF 3DVAR;

GBESM: Same as GBESL, but assimilating both GTS and Korean AWS data (Fig. 2b) in the WRF 3DVAR. The last letter "M" represents the assimilation of METeorological Actual Report (METAR) (AWS) data;

MBESD: Conventional GTS observational data (Fig. 2a) are assimilated via the WRF 3DVAR with the default MM5 BES, followed by a 24-h forecast using the WRF model. The first letter "M" represents MM5;

MBESL: Same as MBESD, but with the tuned scale-lengths of MM5 BES in the WRF 3DVAR;

MBESM: Same as MBESL, but assimilating both GTS and Korean AWS data (Fig. 2b) in the WRF 3DVAR.

All experiments are executed for 24 hours numerical simulation using the WRF model from 0000 UTC 31 August 2002 to 0000 UTC 1 September 2002 with a 3-hour interval output. The boundary conditions for the numerical predictions use the NCEP AVN analysis with a 6-h interval. The model physics are exactly the same in all experiments, which include YSU-PBL, RRTM longwave and Dudhia shortwave radiation schemes, Monin-Obukhov multiple soil layers, Betts-Miller-Janjic cumulus parameterization, and the Lin et al. (1983) explicit microphysics scheme with graupel. The integration time step is 60 seconds.

7. Numerical results

7.1 *Track*

For typhoon forecasts, the main concerns are the track prediction and precipitation forecast. Table 1 lists the position deviations of Rusa's track between simulations and observation every 3 hours. The Rusa observation locations are from the Tokyo Typhoon Center.

From Table 1, it is obvious that the WRF predictions with background error statistics from mesoscale model MM5 (MM5 BES) obtain a better track than those with global error statistics (Global BES). The average position deviations are reduced from 93.8 km in GBESD to 68.0 km in MBESD, from 72.0 km in GBESL to 65.6 km in MBESL, and from 70.7 km in GBESM to 60.5 km in MBESM. This indicates that the background error statistics using the model forecasts with similar resolution and domain via the NMC method are beneficial to the 3DVAR analyses and the subsequent forecast. It is difficult to obtain a sound mesoscale 3DVAR analysis using the global background error statistics.

Table 1. The deviation between simulation and observation of the Rusa position (units: km)

EXPT.	0-h	3-h	6-h	9-h	12-h	15-h	18-h	21-h	24-h	aver.
CNTRL	35.4	44.6	81.8	72.4	110.6	111.8	86.5	136.8	144.3	91.6
GBESD	36.9	43.0	79.6	73.2	129.8	127.9	129.8	113.9	110.2	93.8
GBESL	33.1	30.6	86.5	84.3	93.8	100.7	87.2	75.9	56.1	72.0
GBESM	41.4	30.4	85.2	96.9	101.6	73.6	80.7	73.9	52.6	70.7
MBESD	29.2	32.8	79.9	81.4	91.9	84.2	81.2	77.7	53.6	68.0
MBESL	30.1	31.9	62.0	71.1	93.3	88.7	81.2	78.5	53.8	65.6
MBESM	44.5	40.4	61.9	45.9	67.5	74.9	75.4	78.2	55.7	60.5

Comparing experiment CNTRL with MBESD, we can probe the enhancement of conventional GTS observations (Fig. 2a) in tropical cyclone initialization and numerical prediction. Figure 4 shows the simulated 24-h tracks of Typhoon Rusa at every 3 hours for CNTRL (symbol "C") and MBESD (symbol "G"). The Tokyo Typhoon Center best track (OBS) of typhoon Rusa (symbol "O") is also plotted in the figure for comparison. From the figure and Table 1, we see that the typhoon Rusa initial position of experiment MBESD is better than experiment CNTRL. The landfall location and time of experiment MBESD are closer to the observation than experiment CNTRL. The track after 9 hours in experiment MBESD is also closer to the best track. The average track deviation of experiment MBESD is 23.6 km less than experiment CNTRL. The WRF 3DVAR can extract useful information from conventional GTS observation data in the typhoon initialization and has a positive impact on the numerical prediction.

Figure 5 depicts the difference in wind vector and wind speed (solid lines) between experiment MBESD and experiment CNTRL at the initial time at 500 hPa. The symbol "O" is Typhoon Rusa's observational center. After assimilation of GTS observations, the circulation of typhoon Rusa is intensified. The surrounding wind speed is increased mainly in the northern part of the typhoon. The east wind is strengthened more than 4 m s^{-1} near the tip of the Korean Peninsula. Compared with the Jindo radar image of typhoon Rusa at the same time (Fig. 1), the increase of the east wind speed near the tip of the Korean Peninsula in Fig. 5 is consistent with the radar observations. The assimilation of GTS observations using the WRF 3DVAR results in the strengthening of typhoon circulation, and obtains improvement in the typhoon initialization and subsequent track prediction.

The tuning of scale-lengths in the recursive filter also has an impact on the 3DAVR analysis and subsequent prediction. Figure 6 shows the 24-h forecasted Rusa track by the WRF model at every 3 hours for experiment CNTRL (symbol "C"), GBESD (symbol

"D") and GBESL (symbol "T"). The Tokyo Typhoon Center best track (OBS) of typhoon Rusa (symbol "O") is also shown in the figure for comparison. From the figure and Table 1, we can see that the track in experiment GBESD is worse than experiment CNTRL, and the landfall time of experiment GBESD is delayed by about 3 hours compared with experiment CNTRL. After tuning the scale-lengths of the recursive filter in global BES, the average Rusa position in experiment GBESL improves 21.8 km from experiment GBESD. The typhoon initial position of experiment GBESL is closer to the observation location than experiments GBESD and CNTRL. The landfall position and time of experiment GBESL are also closer to the best track than experiments GBESD and CNTRL. The typhoon movement in GBESL speeds up after 9 hours, which is consistent with the observation. The track in experiment MBESL is also better than the experiment
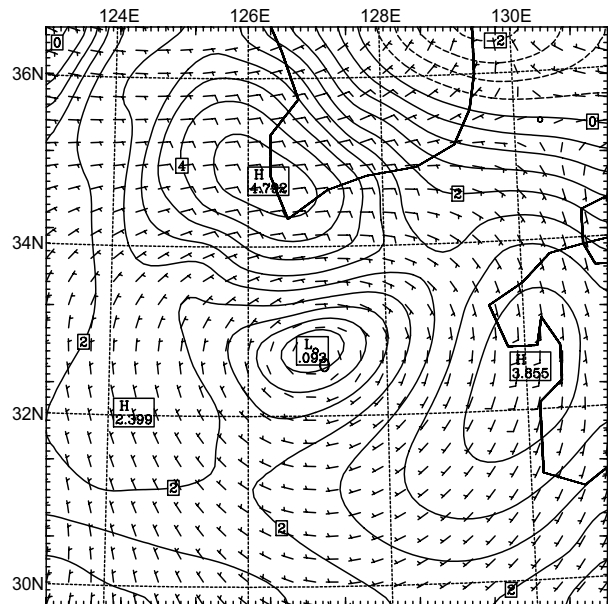
Fig. 5. The difference in wind vector and wind speed (solid; units: m s^{-1}; contour interval: 0.5) between experiment MBESD and experiment CNTRL at initial time at 500 hPa. The symbol "O" is Rusa's observed position.
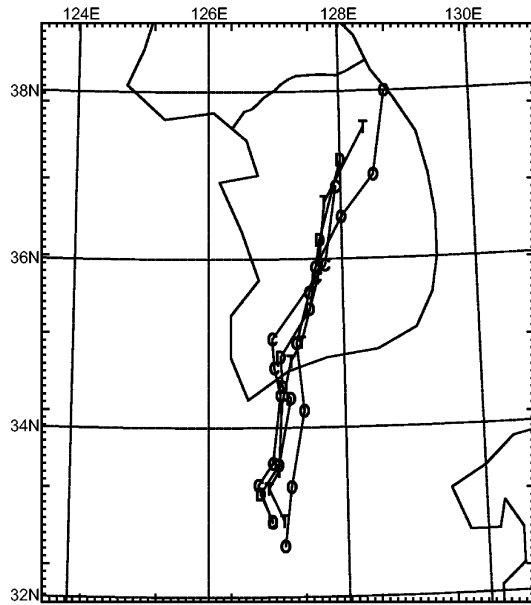
Fig. 6. Typhoon Rusa's simulated and observed tracks. Symbol "O" is the best track; Symbol "C" is the CNTL track; Symbol "D" is the experiment GBESD track; Symbol "T" is the experiment GBESL track.
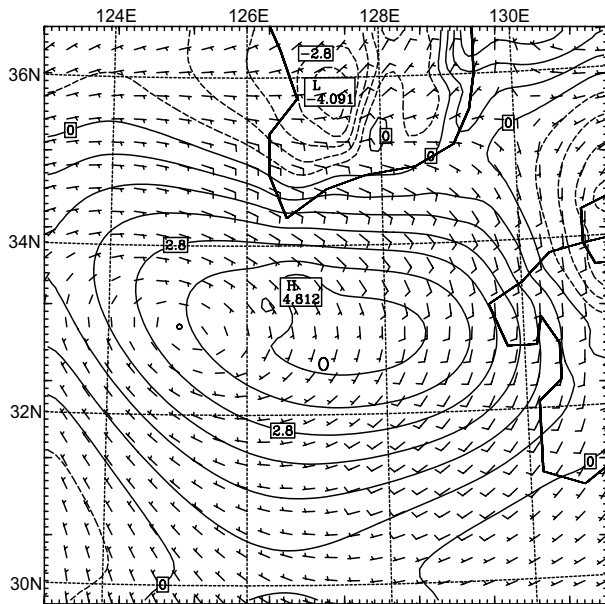

Fig. 7. The difference in wind vector and vertical vorticity (solid, units: s^{-1}, contour interval: 0.7×10^{-5}) between experiment GBESL and experiment GBESD at initial time at 500 hPa. The symbol "O" is Rusa's observed position.

MBESD. This result demonstrates that the tuning of scale-lengths in the recursive filter of the WRF 3DVAR is meaningful to the analysis and subsequent numerical prediction, especially for the global BES.

Figure 7 shows the difference in wind vector and relative vorticity (solid lines) between experiment

GBESL and experiment GBESD at 500 hPa at the initial time. The symbol "O" is Rusa's observational center position. After tuning scale-lengths in the recursive filter, the circulation of typhoon Rusa is intensified. The vertical vorticity is increased around the typhoon region. The southeast wind in the northern part of the typhoon and the south wind in the eastern part of the typhoon are all enhanced. These two regions of wind strengthening (more than 4 m s^{-1}) are also consistent with the radar observations (Fig. 1). The tuning of scale-lengths in the recursive filter of the WRF 3DVAR results in the strengthening of typhoon circulation and gives rise to the improved typhoon initialization and forecast.

In the interest of assessing the assimilation of Korean AWS observations, we inspect the experiments of GBESM versus GBESL, and MBESM versus MBESL. Figure 8 shows that the assimilation of AWS observations (GBESM and MBESM) obtains reduced typhoon track deviation, compared with the experiments GBESL and MBESL, respectively. The experiment GBESM slightly improves the average deviation by 1.3 km; the experiment MBESM improves the average deviation by 5.1 km (Table 1).

7.2 *Precipitation*

Another important interest in typhoon prediction is the inland precipitation forecast at the typhoon's landfall. The U.S. Weather Research Program (USWRP) and World Weather Research Program (WWRP) have identified quantitative precipitation forecasting (QPF) as a major focus of their research on hurricanes at landfall. Therefore the accumulated 24-h precipitation from Korean AWS observations between 0000 UTC 31 August 2002 and 0000 UTC 1 September 2002 (Fig. 9) is used to verify the
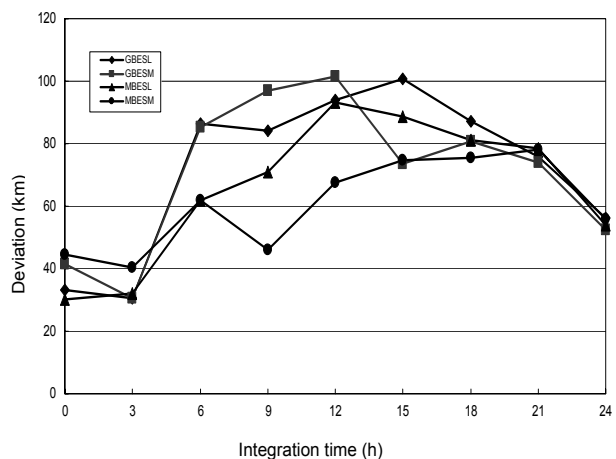

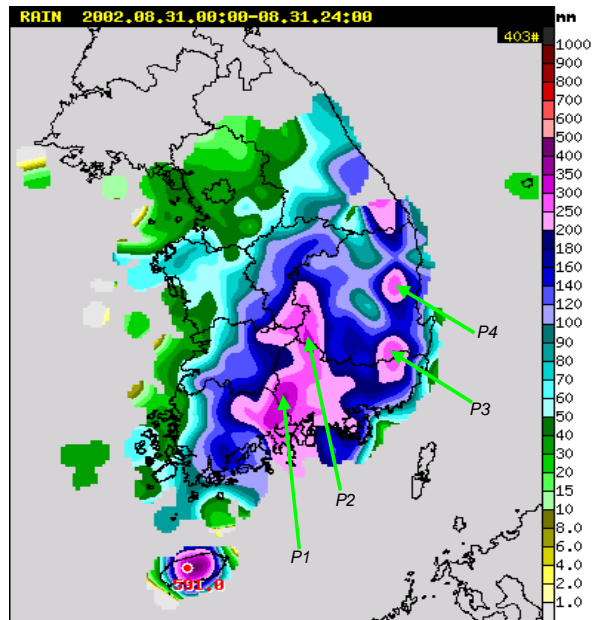**Fig. 8.** The typhoon track deviation of experiments GBESL, GBESM, MBESL and MBESM every 3 hours.

Fig. 9. The observed 24-h accumulation precipitation from 0000 UTC 31 August to 0000 UTC 1 September 2002.

precipitation forecast skill of the designed experiments. The dominant precipitation centers in South Korea are P1 (350 mm), P2 (300 mm), P3 (250 mm) and P4 (250 mm) (Fig. 9). Figure 10 illustrates the 24-h simulation accumulated rainfall distribution for the different experiments. The control experiment (Fig. 10a) can simulation these 4 rainfall centers, but the amounts are apparently less than the observation except for at P4. The deviations of accumulated rainfall between the observation and the experiment CNTRL are 150 mm at P1, 45 mm at P2 and 42 mm at P3.

In order to inspect the effect of the two different BESs in the WRF 3DVAR on the rainfall prediction, we compare experiment GBESD (Fig. 10b) with MBESD (Fig. 10d). It is obvious that the WRF forecast with background error statistics from mesoscale model MM5 (MM5 BES) obtains more intensified simulation precipitation than those with global error statistics (Global BES). The prediction rainfall quantities of experiment MBESD increase 25 mm at P1, 36 mm at P2, and 49 mm at P3; compared to those of experiment GBESD. The simulated precipitations in MBESD are closer to the observation (Fig. 9) than GBSED except for P4. Compared with the observation, the deviations are reduced from 150 mm at P1, 61 mm at P2 and 25 mm at P3 in GBESD to 125 mm at P1, 25 mm at P2 and 24 mm at P3 in MBESD. This indicates that the background error statistics using the model forecasts with similar resolution and domain via the NMC method are beneficial to the typhoon precipitation prediction.

After tuning scale-lengths of the recursive filter in the WRF 3DVAR, the simulated rainfall also increases. Figure 10c shows that the 24-h accumulated precipitations in experiment GBESL are 200 mm at P1, 243.6 mm at P2, 253.8 mm at P3 and 250 mm at P4. The deviations from the observation are reduced from 61 mm at P2 and 25 mm at P3 in GBESD to 56 mm at P2 and 4 mm at P3 in GBESL. This result demonstrates that the tuned scale-lengths can improve the typhoon precipitation prediction.

Comparing the experiments MBESD (Fig. 10d) and CNTRL (Fig. 10a), the assimilation of conventional GTS observations with the WRF 3DVAR also increases the accumulated typhoon precipitation. Figure 10d shows that the 24-h precipitations of the 4 centers in experiment MBESD are 225 mm at P1, 275.4 mm at P2, 273.6 mm at P3 and 308.3 mm at P4. Although the precipitation at P4 is unreasonably large compared to the observation, MBESD simulated the other 3 centers reasonably well. The precipitation differences between observation and experiment MBESD are reduced to 125 mm at P1, 25 mm at P2 and 24 mm at P3.

A more realistic simulation of the precipitation distribution compared to the other experiments is obtained in experiment MBESM (Fig. 10e). Except for P4, the 24-h accumulated precipitations for P1, P2, and P3 are 250 mm, 267.7 mm, and 256 mm, respectively. The deviations of the 24-h accumulated rainfall at these 3 centers between the observation and the experiment MBESM are 100 mm at P1, 32 mm at P2 and 4 mm at P3. Assimilation of Korea AWS data with the tuned scale-lengths of the background error statistics results in an improved skill in precipitation simulation.

8. Summary and conclusions

Using the recently developed the WRF 3DVAR and the WRF model, this paper studied the impact of typhoon initial fields enhanced via scale-length tuning in the recursive filter and assimilation of conventional GTS data and AWS observations upon the subsequent track and precipitation forecasts of typhoon Rusa (2002). The most important results from this study are summarized as follows:

(1) The WRF 3DVAR analyses improve typhoon track and rainfall prediction compared with the experiment without initial data assimilation. The improvements include enhanced typhoon initial circulation, better landfall location and landfall time, and a reasonable forecast rainfall distribution.
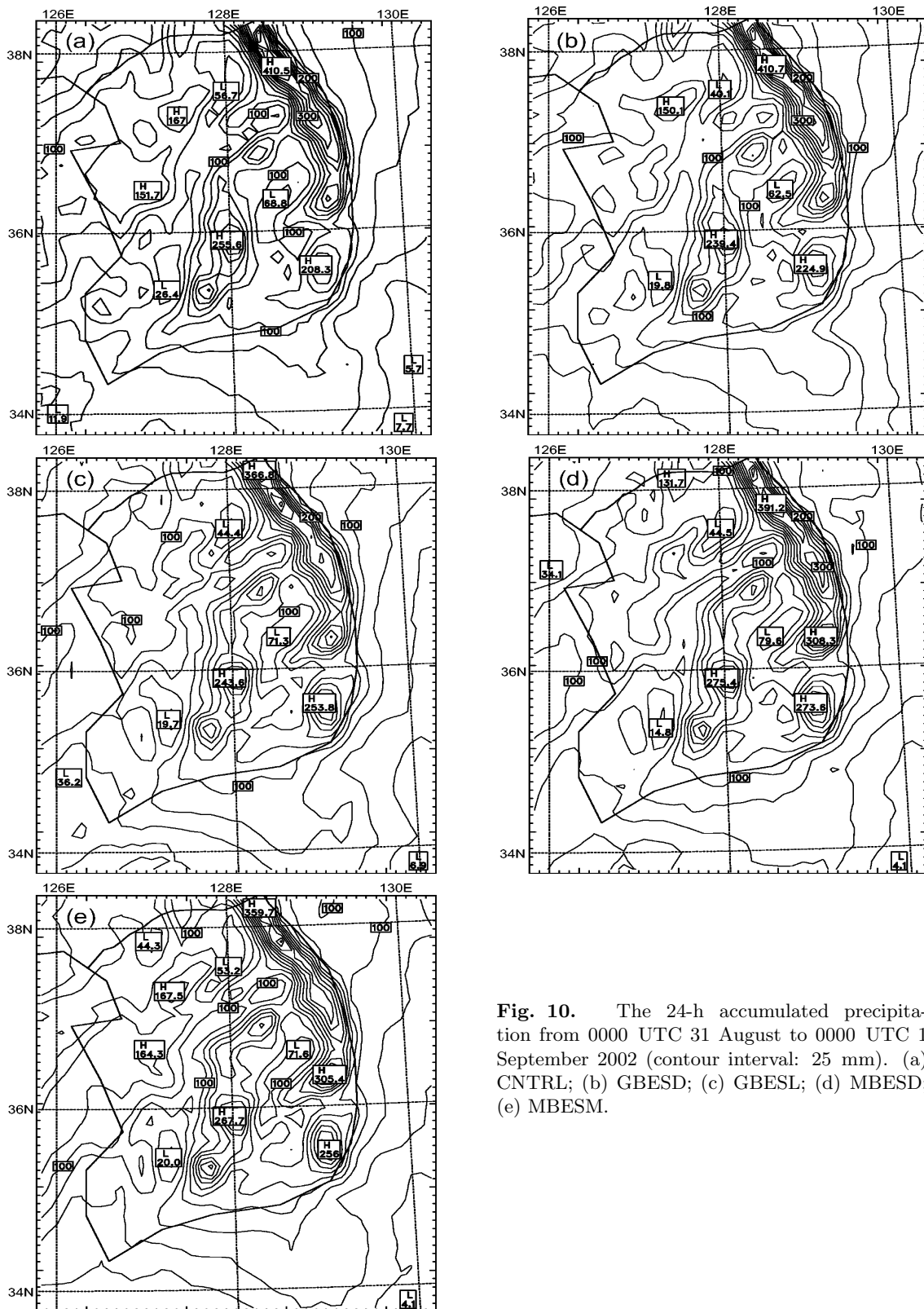
Fig. 10. The 24-h accumulated precipitation from 0000 UTC 31 August to 0000 UTC 1 September 2002 (contour interval: 25 mm). (a) CNTRL; (b) GBESD; (c) GBESL; (d) MBESD; (e) MBESM.

(2) The mesoscale background error statistics which have the same resolution and domain are more suitable for the 3DVAR analyses and subsequent typhoon forecast than the background error statistics from the global model forecast (Global BES).

(3) The scale-length tunings for the 3DVAR recursive filter can significantly improve the typhoon initial structure and the subsequent typhoon track and precipitation forecasts, especially when using global background error statistics. The improvements include strengthening the typhoon initial circulation, better forecasting the landfall location and landfall time, and improving the forecasted rainfall distribution (but the results of precipitation prediction along the Korean northeast coast seem mixed). This result indicates that the background error statistics are a crucial component of the 3DVAR system, allowing the 3DVAR system to more effectively extract useful information from the observations and to improve the typhoon simulation.

(4) Incorporation of extra AWS observations in the assimilation procedure can result in a more realistic simulation of the typhoon-induced inland precipitation distribution and a better typhoon track prediction.

In this paper, we only study the horizontal component of BES. In future work, we will pay attention to studying the vertical and physical components of BES as well as observation errors.

REFERENCES

Barker, D. M., W. Huang, Y.-R. Guo, and Q. Xiao, 2004: A three-dimensional variational (3DVAR) data assimilation system for use with MM5: Implementation and initial results. *Mon. Wea. Rev.*, **132**, 897–914.

Courtier, P., 1985: Experiments in data assimilation using the adjoint model technique. Preprints. *Workshop on High-Resolution Analysis*, Reading, United Kingdom, European Centre for Medium-Range Weather Forecasts, 1–20.

Courtier, P., E. Anderson, W. Heckley, J. Pailleux, D. Vasiljevic, M. Hamrud, A. Hollingsworth, F. Rabier, and M. Fischer, 1998: The ECMWF implementation of three dimensional variational (3DVAR) data assimilation. Part I: Formulation. *Quart. J. Roy. Meteor. Soc.*, **123**, 1–26.

Courtier, P., J. –N. Thepaut, and A. Hollingsworth, 1994: A strategy for operational implementation of 4D-Var, using an incremental approach. *Quart. J. Roy. Meteor. Soc.*, **120**, 1367–1387.

Derber, J. C., 1985: The variational 4-D assimilation of analyses using filtered models as constraints. Ph.D. dissertation, University of Wisconsin-Madison, 142pp.

Hayden, C. M., and R. J. Purser, 1995: Recursive filter objective analysis of meteorological fields: Applications to NESDIS operational processing. *J. Appl. Meteor.*, **34**, 3–15.

Le Dimet, F. X., 1982: A general formalism of variational analysis. CIMMS Rep. 22, 1–34. [Available from Sarkeys Energy Center, Rm 1110, University of Oklahoma, Norman, OK 73019.]

Le Dimet, F. X., and O. Talagrand, 1986: Variational algorithms for analysis and assimilation of meteorological observations: Theoretical aspects. *Tellus*, **38A**, 97–110.

Lewis, J. M., and J. C. Derber, 1985: The use of the adjoint equation to solve a variational adjustment problem with advective constraints. *Tellus*, **37A**, 309–322.

Li, Z., I. M. Navon, and Y. Zhu, 2000: Performance of 4D-var with different strategies for the use of adjoint physics with the FSU global spectral model. *Mon. Wea. Rev.*, **128**, 668–688.

Li, Z., and I. M. Navon, 2001: Optimality of variational data assimilation and its relationship with the Kalman filter and smoother. *Quart, J. Roy. Meteor. Soc.*, **127**, 661–883.

Lin, Y. L., R. D. Farley, and H. D. Orville, 1983: Bulk parameterization of the snow field in a cloud model. *J. Climate Appl. Meteor.*, **22**, 1065–1092.

Lorenc, A. C., 1986: Analysis methods for numerical weather prediction. *Quart. J. Roy. Meteor. Soc.*, **112**, 1177–1194.

Lorenc, A. C., and Coauthors, 2000: The Met. Office global three-dimensional variational data assimilation scheme. *Quart. J. Roy. Meteor. Soc.*, **126**, 2991–3012.

Navon, I. M., X. Zou, J. Derber, and J. Sela, 1992: Variational data assimilation with an adiabatic version of the NMC spectral model. *Mon. Wea. Rev.*, **120**, 1433–1446.

Parish, D. F., and J. Derber, 1992: The National Meteorological Center's spectral statistical-interpolation analysis system. *Mon. Wea. Rev.*, **120**, 1747–1763.

Purser, R. J., W.-S. Wu, D. F. Parrish, and N. M. Roberts, 2003a: Numerical aspects of the application of recursive filters to variational statistical analysis. Part I: Spatially homogeneous and isotropic Gaussian covariances. *Mon. Wea. Rev.*, **131**, 1524–1535.

Rabier, F., A. McNally, E. Anderson, P. Courtier, P. Unden, J. Eyre, A. Hollingsworth, and F. Bouttier, 1997: The ECMWF implementation of three dimensional variational (3DVar) data assimilation. Part II: Structure function. *Quart. J. Roy. Meteor. Soc.*, **123**, 27–52.

Sasaki, Y. 1958: An objective analysis based on variational methods. *J. Meteor. Soc. Japan*, **36**, 77–88.

Talagrand, O., and P. Courtier, 1987: Variational assimilation of meteorological observations with the adjoint vorticity equation–Part I. Theory. *Quart. J. Roy. Meteor. Soc.*, **113**, 1311–1328.

Wu, W.-S., J. Purser, and D. E. Parrish, 2002: Three-dimensional variational analysis with spatial inhomogeneous covariances. *Mon. Wea. Rev.*, **130**, 2905–2916.

Xiao, Q., X. Zou, and B. Wang, 2000: Initialization and simulation of a landfalling hurricane using a variational bogus data assimilation scheme. *Mon. Wea. Rev.*, **128**, 2252–2269.

Xiao, Q., X. Zou, M. Pondeca, M. A. Shapiro, and C. Velden, 2002: Impact of GMS-5 and GOES-9 satellite-derived winds on the prediction of a NORPEX extratropical cyclone. *Mon. Wea. Rev.*, **130**, 507–528.

Zhang, X., B. Wang, Z. Ji, Q. Xiao, and X. Zhang, 2003: Initialization and simulation of a typhoon using 4-dimensional variational data assimilation—Research on typhoon Herb (1996). *Adv. Atmos. Sci.*, **20**(4), 612–622.

Zou, X., I. M. Navon, and J. G. Sela, 1993a: Control of gravitational oscillations in variational data assimila-tion. *Mon. Wea. Rev.*, **121**, 272–289.

Zou, X., I. M. Navon, and J. G. Sela, 1993b: Variational data assimilation with moist threshold processes using the NMC spectral model. *Tellus*, **45A**, 370–387.

Zou, X., and Q. Xiao, 2000: Studies on the initialization and simulation of a mature hurricane using a varia-tional bogus data assimilation scheme. *J. Atmos. Sci.*, **57**, 836–860.

Zupanski, M., 1993: Regional four-dimensional variational data assimilation in a quasi-operational forecasting environment. *Mon. Wea. Rev.*, **121**, 2396–2408.